

The effect of temperature difference on the acoustics performance of Helmholtz resonators

Original article

Article history:

Submission date: 8 December 2023

Acceptance date: 4 May 2024

Publication date: 3 October 2024

This is the updated version of a paper originally presented at the Global Power and Propulsion Technical Conference, GPPS Hong Kong23, October 17–19, 2023.



*Correspondence:

DY: yangd3@sustech.edu.cn

Peer review:

Single blind

Copyright:

© 2024 Gan and Yang © This is an open access article distributed under the Creative Commons Attribution Non Commercial No Derivatives License (CC BY-NC-ND 4.0). Unrestricted use, distribution, and reproduction of the original work are permitted for noncommercial purposes only, provided it is properly cited and its authors credited. No derivative of this work may be distributed.

Keywords:

temperature difference; thermoacoustic instability; cooling bias flow; acoustic analogy; Helmholtz resonator

Citation:

Gan Z., Yang D. (2024). The effect of temperature difference on the acoustics performance of Helmholtz resonators. *Journal of the Global Power and Propulsion Society*, 8: 349–359.
<https://doi.org/10.33737/jgpps/188265>

Zhenpeng Gan¹, Dong Yang^{1*}

¹*Southern University of Science and Technology, 1088 Xueyuan Blvd, Nan Shan Qu, Shenzhen, Guangdong 518055, China*

Abstract

Passive control devices such as liners and Helmholtz resonators (HRs) are commonly employed in practical applications to mitigate thermoacoustic instabilities. To safeguard the HR from being corroded by the invasion of hot flow from the combustor, a cooling flow with significantly lower temperature than that in the combustor is injected from the rear of the HR cavity. However, this results in a dynamic mixing of cold bias and hot grazing flows in the combustor, which may generate an entropy wave downstream of the HR, thereby affecting its sound absorption performance. Unfortunately, these effects are often neglected when modelling such systems. In this context, an acoustic model is derived for a one-dimensional combustor duct with distinct temperature compared to that of the attached HR. The model offers physical insights into the underlying mechanisms of the impact of HR on the acoustic fields. It considers not only the mean temperature difference between the cooling bias flow and the main flow in the combustor, but also the mean temperature difference between the up- and downstream sides of the combustor across the HR. The effect of both temperature differences on the HR's performance will be discussed.

Introduction

Lean premixed combustion is widely utilized to minimize the emission of NO_x by reducing the peak temperature within combustor, while simultaneously maintaining low levels of other pollutants (Correa, 1998; Lewis et al., 1999; Lefebvre and Ballal, 2010). However, the combustion process in lean premixed systems is highly sensitive to noise disturbances, which can lead to undesirable thermoacoustic instability (Poinsot, 2017). Thermoacoustic instability is a challenging problem in many combustion systems especially in gas turbine combustors, which can result in high-amplitude pressure oscillations leading to loud noise, reduced efficiency, and even risks of structural damage. This instability arises from the coupling between acoustic waves and heat release fluctuations within the system, causing pressure oscillations that can grow in amplitude and cause combustor instability. Passive control methods have been proposed as a promising means to mitigate thermoacoustic instability without requiring major modifications to combustion system hardware. One of such technologies is the Helmholtz resonator, which works by absorbing acoustic energy, thereby disrupting the coupling between acoustic waves and pressure fluctuations in the combustor.

When analyzing the performance of a Helmholtz resonator in suppressing thermoacoustic instability, an isolated description of damper behavior is insufficient and requires investigation of the coupled system

neck region, and thus, there is no occurrence of hot grazing flow intrusion, i.e. $T_{HR} = T_n$. In this study, we make certain assumptions, including (i) considering fluids in the system as single-component ideal gases using the gas law $p = R_{gas}\rho T$, (ii) neglecting body forces, any heat addition and thermal diffusion, (iii) ignoring viscosity in the main body of the fluid except for near the HR neck region, where its effect is considered by using a HR model, (iv) assuming small perturbation amplitudes resulting in a linear system, (v) considering only plane waves in the combustor duct due to the low frequency (due to the low frequency of combustion instabilities, typically below 1 kHz, the dominant mode is often the plane wave mode) (Lieuwen and Yang, 2005).

Governing equation

The conservation of mass, momentum and energy for this one-dimension combustion duct gives

$$A_c \left(\frac{\partial \rho}{\partial t} + \frac{\partial(\rho u)}{\partial x} \right) = \delta(x_b) \dot{m}, \quad (1a)$$

$$A_c \left(\frac{\partial(\rho u)}{\partial t} + \frac{\partial(u^2 \rho + p)}{\partial x} \right) = \delta(x_b) \dot{f}, \quad (1b)$$

$$A_c \left(\frac{\partial[\rho(C_p T + 0.5u^2)]}{\partial t} + \frac{\partial[\rho u(C_p T + 0.5u^2)]}{\partial x} \right) = \delta(x_b) \dot{e}, \quad (1c)$$

where C_p is the heat capacity at constant pressure which is in general a function of temperature, ρ the fluid density, $\delta(x)$ the Dirac delta function, \dot{m} the mass flux source term coming from the HR, \dot{f} the momentum flux source term coming from the HR (assuming that the neck flux is radially inwards with the combustor, so the momentum in the x-direction inside the combustor is constant, i.e., $\dot{f} = 0$) and \dot{e} the energy flux source term coming from the HR. The installation position of the HR is represented by x_b , here $x_b = 0$.

Integrating Equation. (1) from sections 1–2 yields the mean flow conservation equations. Then by giving mean flow parameters upstream the resonator, $\bar{\rho}_1$, \bar{u}_1 and \bar{T}_1 , and combining perfect gas relation, the mean flow parameters downstream the HR, $\bar{\rho}_2$, \bar{u}_2 , \bar{p}_2 and \bar{T}_2 , can be obtained. To obtain the acoustic governing equation, we linearize Equations. (1a) and (1b), subtract their respective mean quantity equations and keep only the first-order perturbation terms (due to the linear system), resulting in

$$\frac{\partial \rho'}{\partial t} + \rho' \frac{\partial \bar{u}}{\partial x} + \bar{\rho} \frac{\partial u'}{\partial x} + u' \frac{\partial \bar{\rho}}{\partial x} + \bar{u} \frac{\partial \rho'}{\partial x} = \frac{\delta(x_b) \dot{m}'}{A_c}, \quad (2)$$

$$\bar{u} \frac{\partial \rho'}{\partial t} + \bar{\rho} \frac{\partial u'}{\partial t} + \frac{\partial}{\partial x} (\bar{u}^2 \rho') + 2 \frac{\partial}{\partial x} (u' \bar{u} \bar{\rho}) + \frac{\partial p'}{\partial x} = 0. \quad (3)$$

Due to the dynamic mixing of cold and hot flows, the system will naturally generate entropy waves. Therefore, the density perturbation will include the effect of entropy perturbations $\rho' = p'/\bar{c}^2 - s'\bar{\rho}/C_p$. By taking the derivative of Equation (2) with respect to time t, subtracting the derivative of Equation (3) with respect to space x, we can obtain

$$\frac{\partial^2 \rho'}{\partial t^2} - \frac{\partial^2}{\partial x^2} (\bar{u}^2 \rho') - \frac{\partial^2}{\partial x^2} (2\bar{u}\bar{\rho}u') - \frac{\partial^2 p'}{\partial x^2} = \frac{\delta(x_b)}{A_c} \frac{\partial \dot{m}'}{\partial t}. \quad (4)$$

This is our one-dimensional acoustic wave governing equation.

In order to obtain the relation between the up- and downstream pressure disturbances, Equation (4) needs to be solved. Equation (4) degenerates to a homogeneous equation in the regions up- and downstream of the HR (in $x < 0$ and $x > 0$ respectively), where the general solutions can be written as

$$\tilde{p}_1 = \tilde{p}_1^+ e^{-ik_1^+ x} + \tilde{p}_1^- e^{ik_1^- x}, \quad \tilde{p}_2 = \tilde{p}_2^+ e^{-ik_2^+ x} + \tilde{p}_2^- e^{ik_2^- x}, \quad (5)$$

where $\tilde{[p]}$ denotes the Fourier amplitude, k^+ and k^- denote the wavenumber

$$k_{1,2}^+ = \frac{\omega}{\bar{c}_{1,2} + \bar{u}_{1,2}}, \quad k_{1,2}^- = \frac{\omega}{\bar{c}_{1,2} - \bar{u}_{1,2}}, \quad (6)$$

By integrating once and twice of Equation (4) with respect to x across the source region, substituting the wave number Equation (6) and the expression for density disturbance $\rho' = p'/\bar{c}^2 - s'\bar{\rho}/C_p$, we can obtain

$$\frac{(1 + \bar{M}_2)^2}{\bar{c}_2 + \bar{u}_2} \tilde{p}_2^+ - \frac{(1 - \bar{M}_2)^2}{\bar{c}_2 - \bar{u}_2} \tilde{p}_2^- - \frac{(1 + \bar{M}_1)^2}{\bar{c}_2 + \bar{u}_2} \tilde{p}_1^+ + \frac{(1 - \bar{M}_1)^2}{\bar{c}_2 - \bar{u}_2} \tilde{p}_1^- = \frac{\bar{\rho}_2 \bar{u}_2}{C_{p2}} \tilde{s}_2 + \frac{\tilde{m}_n}{A_c}, \tag{7}$$

$$(1 + \bar{M}_2)^2 \tilde{p}_2^+ + (1 - \bar{M}_2)^2 \tilde{p}_2^- - (1 + \bar{M}_1)^2 \tilde{p}_1^+ - (1 - \bar{M}_1)^2 \tilde{p}_1^- = \frac{\bar{\rho}_2 \bar{u}_2^2}{C_{p2}} \tilde{s}_2. \tag{8}$$

We note that integrating $\tilde{m}(x)\delta(x_b)$ over x gives the mass flux perturbation from the HR, i.e., \tilde{m}_n , which can be related to the pressure perturbation at the neck outlet, \tilde{p}_1 , through a linear HR model based on the Rayleigh conductivity (Howe, 1979)

$$\tilde{m}_n = \tilde{p}_1 \mathcal{F}, \tag{9}$$

where $\mathcal{F} = -1/(\bar{c}_v^2/(i\omega V) + i\omega/K_R^t)$, V denote the the HR cavity volume, \bar{c}_v sound speed in the HR cavity, ω the angular frequency, K_R^t the revised Rayleigh conductivity defined in references (Eldredge and Dowling, 2003; Rupp et al., 2010; Scarpato et al., 2012). Entropy perturbation \tilde{s} is unknown and can be obtained by combining \tilde{m}_n with the mass and energy equations. We derive the expression for \tilde{s} in the next section.

Entropy model

In order to obtain the oscillating entropy \tilde{s}_2 , we linearise Equations. (1a) and (1c) and take the Fourier transform to give

$$\tilde{m}_1 + \tilde{m}_n = \tilde{m}_2, \quad (\bar{m}_2 + \tilde{m}_2)(\bar{E}_2 + \tilde{E}_2) = (\bar{m}_1 + \tilde{m}_1)(\bar{E}_1 + \tilde{E}_1) + (\bar{m}_n + \tilde{m}_n)(\bar{E}_n + \tilde{E}_n). \tag{10}$$

where $\bar{E} = C_p \bar{T} + (1/2)\bar{u}^2$ denotes the mean stagnation enthalpy, with \tilde{E} the stagnation enthalpy perturbation. By combining Equation (10), the thermodynamic relation $\tilde{T} = (\tilde{s} + R\tilde{p}/\bar{p})\bar{T}/C_p$ and neglecting the second and higher order perturbations and assuming that the entropy perturbation upstream the HR inside the combustor is zero ($\tilde{s}_1 = 0$), we get

$$\tilde{S}_2 = \frac{1}{\bar{T}_2 \bar{m}_2} \{ \tilde{m}_1 \Delta \bar{E}_{12} + \tilde{m}_n \Delta \bar{E}_{n2} + A_c (\bar{u}_1 \tilde{p}_1 - \bar{u}_2 \tilde{p}_2) + (\bar{m}_1 \bar{u}_1 \tilde{u}_1 - \bar{m}_2 \bar{u}_2 \tilde{u}_2) + \bar{m}_n \tilde{E}_n \}, \tag{11}$$

where $\Delta \bar{E}_{12} = \bar{E}_1 - \bar{E}_2$, $\Delta \bar{E}_{n2} = \bar{E}_n - \bar{E}_2$. In this case, small terms of orders higher than or equal to $O(\bar{M}_1)$ (e.g., $\bar{u}_1 \tilde{p}_1 / (\bar{\rho}_1 \tilde{u}_1) \sim O(\bar{M}_1) \ll 1$) can be neglected, due to the low mean flow Mach number in the combustor. Then, the expression of entropy perturbation comes to

$$\tilde{S}_2 \stackrel{\bar{M}_1 \ll 1}{\approx} \frac{1}{\bar{T}_2 \bar{m}_2} \{ \tilde{m}_1 \Delta \bar{E}_{12} + \tilde{m}_n \Delta \bar{E}_{n2} \} \approx \frac{1}{\bar{T}_2 \bar{m}_2} \{ A_c \bar{\rho}_1 \tilde{u}_1 \Delta \bar{E}_{12} + \tilde{m}_n \Delta \bar{E}_{n2} \}, \tag{12}$$

This expression demonstrates that the perturbation of entropy observed in the downstream section of the combustor depends on two factors, namely the variance in the mean stagnation enthalpy between the up-and down-stream sections of the combustor as well as between the HR and downstream section of the combustor.

We have formulated a set of six equations, namely Equations (5), (7)–(9) and (11) with eight unknown perturbation parameters denoted by \tilde{p}_1 , \tilde{p}_2 , \tilde{p}_1^+ , \tilde{p}_1^- , \tilde{p}_2^+ , \tilde{p}_2^- , \tilde{m}_n and \tilde{s}_2 . Combining Equations (5), (7)–(9) and

(11) and reorganizing them into a matrix form, we have

$$\underbrace{\begin{bmatrix} \frac{(1 + \bar{M}_2)^2}{\bar{c}_2 + \bar{u}_2} & -\frac{(1 - \bar{M}_2)^2}{\bar{c}_2 - \bar{u}_2} & -\frac{\bar{\rho}_2 \bar{u}_2}{C_{p2}} \\ (1 + \bar{M}_2)^2 & (1 - \bar{M}_2)^2 & -\frac{\bar{\rho}_2 \bar{u}_2^2}{C_{p2}} \\ A_c \bar{u}_2 (1 + \bar{M}_2) & A_c \bar{u}_2 (1 - \bar{M}_2) & \bar{T}_2 \bar{m}_2 \end{bmatrix}}_{B_1} \begin{bmatrix} \tilde{p}_2^+ \\ \tilde{p}_2^- \\ \tilde{s}_2 \end{bmatrix} = \underbrace{\begin{bmatrix} \frac{(1 - \bar{M}_1)^2}{\bar{c}_1 - \bar{u}_1} + \frac{\mathcal{F}}{A_c} & -\frac{(1 - \bar{M}_1)^2}{\bar{c}_1 - \bar{u}_1} + \frac{\mathcal{F}}{A_c} \\ (1 + \bar{M}_1)^2 & (1 - \bar{M}_1)^2 \\ A_c \bar{u}_1 (1 + \bar{M}_1) + \frac{A_c}{\bar{c}_1} \Delta \bar{E}_{12} + \mathcal{F} (\Delta \bar{E}_{n2} + \bar{u}_n^2 + A_n \bar{u}_n) & A_c \bar{u}_1 (1 - \bar{M}_1) - \frac{A_c}{\bar{c}_1} \Delta \bar{E}_{12} + \mathcal{F} (\Delta \bar{E}_{n2} + \bar{u}_n^2 + A_n \bar{u}_n) \end{bmatrix}}_{B_2} \begin{bmatrix} \tilde{p}_1^+ \\ \tilde{p}_1^- \end{bmatrix}, \tag{13}$$

To ensure that the system is well-defined, two boundary conditions must be imposed. Typically, the boundary condition for the inlet and outlet are fixed. If \tilde{p}_1^+ and \tilde{p}_1^- are given, we can then obtain the solution when there is a discontinuity in the mean flow parameters inside the combustor up- and downstream the HR

$$\begin{bmatrix} \tilde{p}_2^+ \\ \tilde{p}_2^- \\ \tilde{s}_2 \end{bmatrix} = B_1^{-1} B_2 \begin{bmatrix} \tilde{p}_1^+ \\ \tilde{p}_1^- \end{bmatrix}. \tag{14}$$

We designate the solution of the acoustic analogy model considering mean flow discontinuity between the up- and downstream of the combustor as MAA. In the subsequent section, we will consider a test case with given boundary condition, and use the Linearized Navier-stokes (LNS) solver in COMSOL to validate the results.

Numerical simulation

To validate the theoretical model, numerical simulations were employed, considering non-steady, compressible, and non-isentropic characteristics to accurately depict information from a three-dimensional flow field. This can be achieved by creating a 3D model of a Helmholtz resonator and combustor duct using COMSOL Multiphysics. The mean flow field results obtained from Computational Fluid Dynamics (CFD) are utilized as the background mean flow. The type of CFD simulation employed in this study is the Reynolds-Averaged Navier-Stokes (RANS) model. These results are inserted into the acoustic mesh using a dedicated mapping module to solve the linearized Navier-Stokes (LNS) equations in the frequency domain. The LNS and CFD governing equations employed in this study are consistent with those described in references (Lu et al., 2019; Wu and Guan, 2021; Dastourani and Bahman-Jahromi, 2021; Zheng et al., 2023). The solution methodology employed in the present simulation adheres to a flowchart, depicted in Figure 2.

Table 1 presents the relevant fluid parameters utilized in both theoretical analysis and numerical simulations, as well as the geometric dimensions of the HR and combustor duct. Figure 3 shows a schematic view of the 3D model, L_{PML} represents the length of the perfect match layer used at both ends of the duct, L_b is the length of the background sound field area, L_{in} and L_{out} the length of flow field upstream and downstream the HR respectively, D_{com} the diameter of the combustor duct, D_{neck} the neck diameter of HR, L_{neck} the neck length, D_{res} both the diameter and height of the HR cavity. The boundary conditions applied for CFD calculations include a fully developed flow at the inlet and a pressure outlet. Additionally, a no-slip condition is imposed on the walls. On the other hand, for the acoustic calculations, the boundary conditions are as follows: the mechanical condition is set as slip, and the thermal condition is set as adiabatic. At the inlet and outlet, the perfectly matched layer (PML) boundary domain is used. The PML acts as a non-reflecting boundary condition, minimizing reflections of acoustic waves. Similar boundary conditions are detailed in (Dastourani and Bahman-Jahromi, 2021).

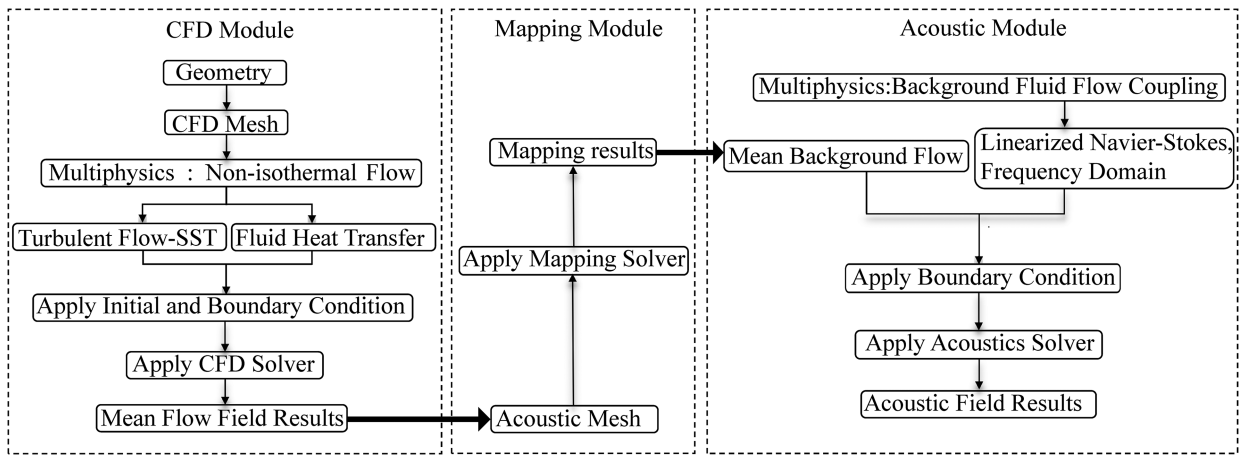


Figure 2. The processes involved in the numerical model of COMSOL.

Table 1. The geometries and flow conditions of the coupled HR-combustor model.

Parameters	Values	Parameters	Values
L_{neck}/cm	0.5	V/m^3	2.5×10^{-4}
L_{PML}/cm	10	A_n/m^2	1×10^{-4}
L_b/cm	10	\bar{T}_n/K	500
L_{in}/cm	60	\bar{T}_1/K	1,000
L_{out}/cm	100	\bar{p}_1/MPa	2
D_{com}/cm	6	\bar{M}_1	0.03
D_{res}/cm	100	\bar{M}_n	$0.03 \rightarrow 0.06 \rightarrow 0.09$

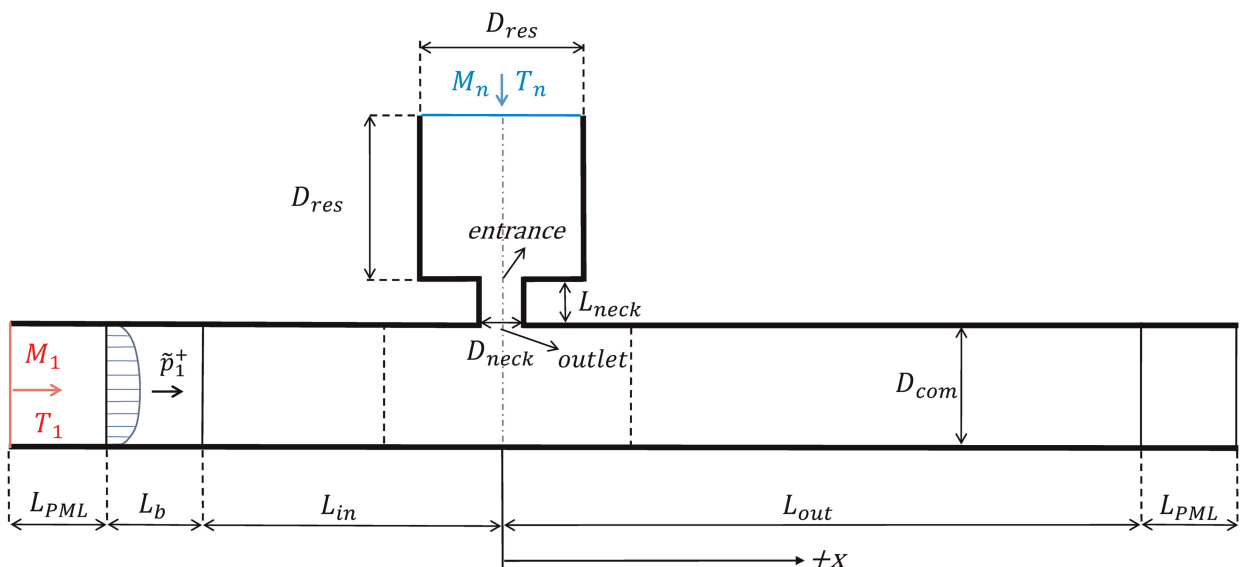


Figure 3. The schematic view of 3D coupled model in COMSOL.

Mesh independence and verification test

In order to validate the accuracy of the modeling approach, the geometric parameters of the model were adjusted to match those used in the experimental (Selamet et al., 2011). The simulated transmission loss results were then compared with the experimental results, as illustrated in Figure 4. To validate the mesh independence of the results in the flow simulations, three meshes with different number of elements were employed, with a total of $Mesh_{c1} = 841, 455$, $Mesh_{c2} = 1, 363, 549$ and $Mesh_{c3} = 1, 856, 129$ elements respectively. The investigation of mesh independence revealed that the computational results from the latter two meshes of CFD (the three meshes of Acoustics) exhibited convergence and were generally consistent, as shown in Figure 5. Two different meshes, comprising $Mesh_{c2} = 1, 363, 549$ and $Mesh_{a2} = 576, 381$ elements, were selected ultimately for the computational fluid dynamics (CFD) and acoustic simulations respectively, as depicted in the Figures 6(a) and 6(b).

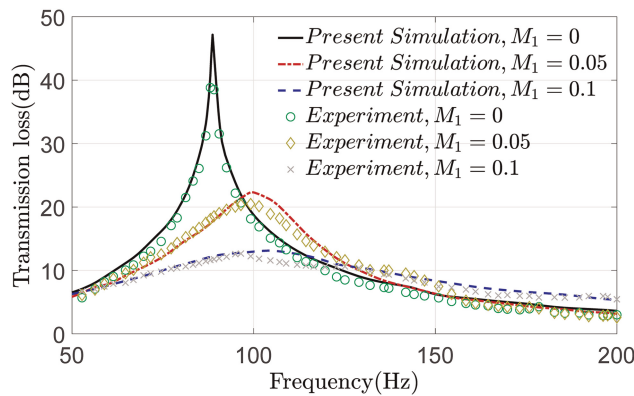


Figure 4. The comparison between the simulated transmission loss (TL) obtained from the model constructed using the current steps in COMSOL and the experimental results.

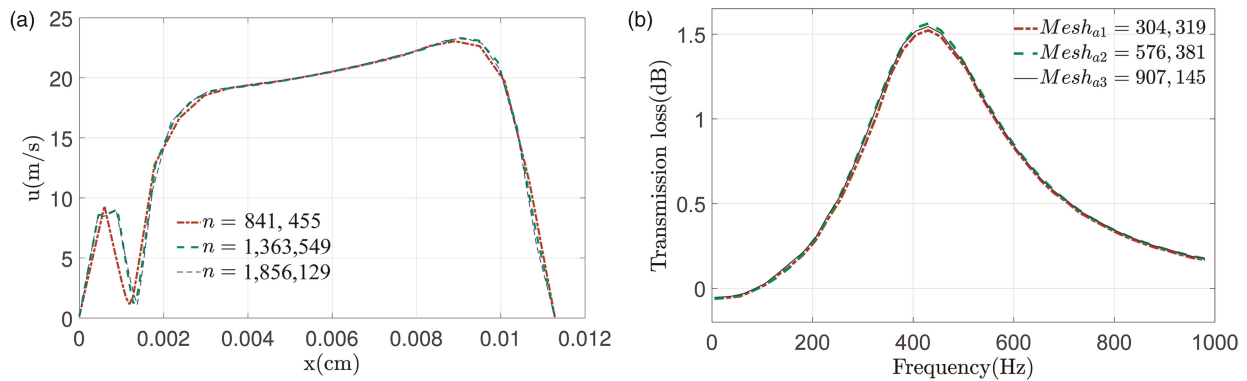


Figure 5. Mesh independence test. (a) Velocity profiles at the $x=D_{(res)}/2$ section of downstream combustor duct for the various CFD meshes. (b) Transmission loss for the various Acoustics meshes.

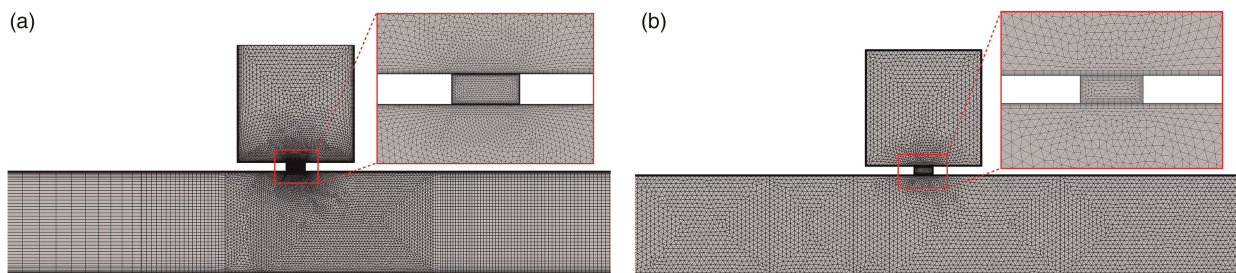


Figure 6. The flow and acoustic meshes utilized for three-dimensional modeling of the coupling of a Helmholtz resonator and combustor. (a) The flow computational mesh. $Mesh_{c2} = 1,363,549$. (b) The acoustics computational mesh. $Mesh_{a2} = 576,381$.

Results and discussion

We now consider a test case to study the effect of the temperature difference between the HR and combustor on the acoustics inside the combustor. In this case, we make the assumption that the upstream and downstream sections of the combustor duct are both infinitely long, i.e. non-reflecting boundary condition. An incident wave $\tilde{p}_1^+ = 100 Pa$ is introduced at the upstream section to excite the entire acoustic field within the combustor.

Comparisons with previous models are performed to validate the present model in the isothermal case. Other different acoustic boundary conditions are also can consider to our model. Maintaining the bias flow temperature $\bar{T}_n = 500K$ and the grazing flow temperature $\bar{T}_1 = 1000K$, we continuously increase bias flow Mach number \bar{M}_n . This is to make the mean bias flow no longer negligible compared to the mean grazing flow. Figures 7 and 8 show the theoretical and COMSOL numerical results for acoustic and transmission loss (defined as $20 \log_{10}|\tilde{p}_1^+/\tilde{p}_2^+|$) with the bias flow Mach numbers set to $\bar{M}_n = 0.03$, $\bar{M}_n = 0.06$, $\bar{M}_n = 0.09$ (corresponding to $\bar{m}_n/\bar{m}_1 \approx 5.1\%$, $\bar{m}_n/\bar{m}_1 \approx 10.2\%$, $\bar{m}_n/\bar{m}_1 \approx 15.3\%$, respectively).

From Figures 7(a) and 8(a), it can be seen that when $\bar{m}_n/\bar{m}_1 \approx 5.1\%$ the prediction results of the AA, MAA, and JC theoretical models are consistent with COMSOL, indicating that the difference in the mean flow parameters before and after crossing the HR can still be ignored, and its effect on the acoustics is negligible. From Figures 7(b) and 8(b), it can be observed that when $\bar{m}_n/\bar{m}_1 \approx 10.2\%$, the predicted results of the AA model differ significantly from those of the MAA and JC models, and the relative error of the peak transmission loss of the AA model based on COMSOL reached 23%, indicating that ignoring the difference in mean flow parameters before and after the HR will affect the accuracy of the results. The numerical results validate the accuracy of the MAA and JC models. When further increasing the bias flow Mach number to $\bar{m}_n/\bar{m}_1 \approx 15.3\%$, the predicted relative error in transmission loss by the AA model is further amplified, reaching approximately 70%, as shown in Figures 7(c) and 8(c). The results of the SEC model demonstrate that these two temperature differences in all three configurations of bias flow Mach numbers should not be overlooked; its predicted outcomes are

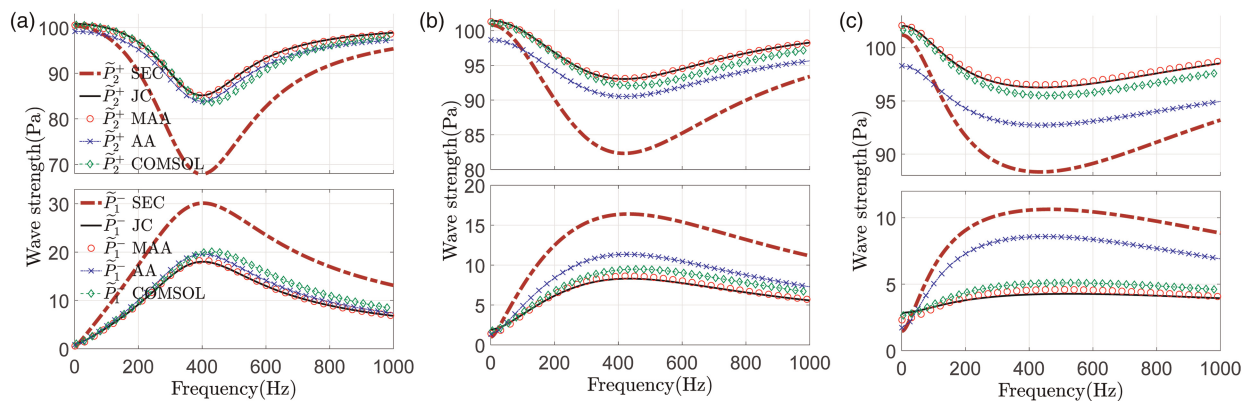


Figure 7. Comparison of acoustic wave strength across various models and numerical results. (a) $\bar{M}_n = 0.03$, $\bar{m}_n/\bar{m}_1 \approx 5.1\%$. (b) $\bar{M}_n = 0.06$, $\bar{m}_n/\bar{m}_1 \approx 10.2\%$. (c) $\bar{M}_n = 0.09$, $\bar{m}_n/\bar{m}_1 \approx 15.3\%$.

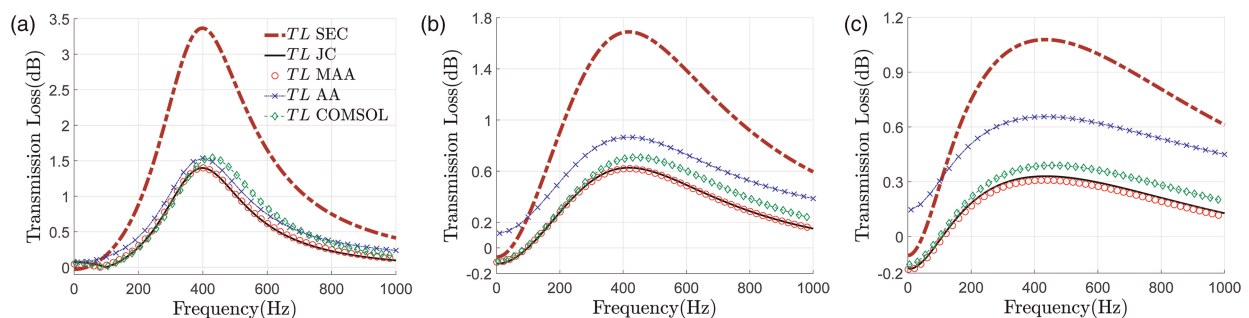


Figure 8. Comparison of downstream duct transmission loss across various models and numerical results. (a) $\bar{M}_n = 0.03$, $\bar{m}_n/\bar{m}_1 \approx 5.1\%$. (b) $\bar{M}_n = 0.06$, $\bar{m}_n/\bar{m}_1 \approx 10.2\%$. (c) $\bar{M}_n = 0.09$, $\bar{m}_n/\bar{m}_1 \approx 15.3\%$.

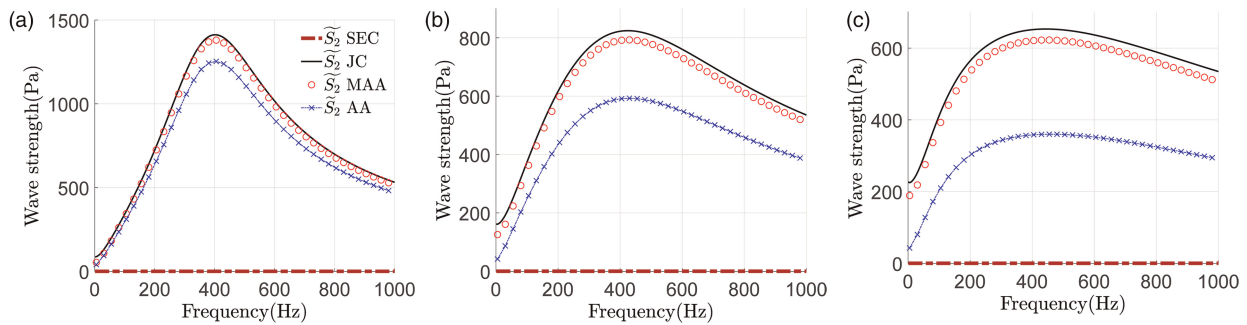


Figure 9. Comparison of entropy wave strength across various models. (a) $\bar{M}_n = 0.03$, $\bar{m}_n/\bar{m}_1 \approx 5.1\%$. (b) $\bar{M}_n = 0.06$, $\bar{m}_n/\bar{m}_1 \approx 10.2\%$. (c) $\bar{M}_n = 0.09$, $\bar{m}_n/\bar{m}_1 \approx 15.3\%$.

significantly different from the current model's predictions. It can be clearly seen that the present MAA model predicts results that are essentially consistent with the numerical simulation in all three cases, with negligible differences. This difference arises from the intrusion of hot grazing flow in the HR neck region in the COMSOL model, leading to an increase in the mean neck temperature. We found that by adjusting the neck input temperature of the theoretical model to match that in COMSOL, the results of the theoretical model perfectly align with those of the COMSOL model. The AA model accounts for the temperature difference in the mean flow between HR and combustor but neglects temperature variations in the mean flow within the combustor upstream and downstream, which can be referenced to our previous work (Gan and Yang, 2022), so cannot predict the correct results when \bar{M}_n is large. The JC model (Yang and Morgans, 2017) correlates the perturbations upstream and downstream via a scattering matrix and, being similar to the present model, can capture the effects of two temperature differences. However, unlike the AA and MAA models, it fails to provide a satisfactory physical interpretation. The SEC model (Dupère and Dowling, 2005) which assumes continuity of stagnation enthalpy between the up- and downstream regions of the combustor, can not capture the two kinds of temperature difference.

The entropy wave strength can be defined as $\tilde{S}(x) = \tilde{s}(x)(\gamma - 1)\bar{\rho}\bar{T}$, where $\tilde{s} = C_v\tilde{p}/\bar{p} - C_p\tilde{\rho}/\bar{\rho}$ represents the entropy disturbance. The predicted curve for the entropy wave strength are shown in Figure 9. Comparison of the AA model with MAA and JC reveals that neglecting the difference in the mean grazing flow across the HR underestimates the generation of entropy wave strength downstream of the combustor. The error of the AA model is small when $\bar{M}_n = 0.03$, while for bias flow Mach numbers up to 0.09, the predicted value of the AA model is half of the MAA and JC models. The observed discrepancy is precisely ascribed to the first term within the parentheses of Equation (12). This term arises from the discontinuity in the mean stagnation enthalpy between the upstream and downstream sides of the combustor.

Conclusion

In this paper, we extend our previous work on the acoustic analogy (AA) model (Gan and Yang, 2022) and propose a new model, MAA. The new model incorporates the effects of temperature difference between the upstream and downstream sides of the combustor in addition to the previously considered effects of temperature difference between the HR and the combustor. While the AA model provides a reasonable explanation for the acoustic effects in the combustor produced by the HR with cooling flow, the new MAA model is more general and includes the discontinuity effects of the mean flow parameters between the upstream and downstream regions of the combustion chamber. Comparing the theoretical and numerical results obtained from the COMSOL simulation, we find that when the ratio between the mean bias mass flux and the mean grazing mass flux does not exceed 10% in this study, the discontinuity effects of the mean flow parameters inside the combustor significantly will have negligible impact on acoustic and entropy wave strengths in the combustor. When this mass ratio is relatively large, ignoring this effect would result in overestimating the transmission loss in the combustor duct and underestimating the entropy waves strength generated downstream of the combustor. Moreover, the error increases with the increase of the bias mass flow rate. Therefore, in some cases where a large bias mass flow rate is required, it is necessary to consider both the temperature difference between the HR and the combustor and the temperature difference between the upstream and downstream regions of the combustor.

Nomenclature

C_p	heat capacity at constant pressure, J/(K · kg)
R_{gas}	the perfect gas constant
K_R^t	Revised Rayleigh conductivity
$\delta(x)$	Dirac's delta function
D	Dimeter, m
L	Length, m
A	Cross-sectional area, m ²
V	The volume of the HR cavity, m ³
m	Mass flux, kg/s
f	Momentum flux, kg·m/s ²
e	Energy flux, kg·m ² /s ³
E	Stagnation enthalpy, J/kg
p	Pressure, Pa
s	Entropy, J/(K·kg)
S	Entropy oscillations strength, Pa
t	Time, s
x	Axial location, m
T	Temperature, K
u	Velocity, m/s
c	Speed of sound, m/s
ω	Angular frequency, rad/s
ρ	Density, kg/m ³
k	The wavenumber, m ⁻¹
M	Mach number
γ	Heat capacity ratio

Abbreviations

<i>SEC</i>	The Dupère and Dowling's Stagnation Enthalpy Continuity model
<i>JC</i>	The Yang and Morgans's Jump Condition model
<i>AA</i>	The Acoustic Analogy model
<i>MAA</i>	The Mean Acoustic Analogy model

Subscripts

n	Neck of the HR
v	Cavity of the HR
$1, 2$	Section number of the system (here a combustor duct)

Superscripts

+	Downstream propagation
–	Upstream propagation
'	Time domain oscillation

Overscripts

\sim	Fourier amplitude of oscillation
–	Mean value

Funding sources

The authors would like to thank the National Natural Science Foundation of China (project No. 52106159) and the Science Center for Gas Turbine Project of China (No. P2022-B-P-013-001) for supporting this research.

Competing interests

Zhenpeng Gan declares that he has no conflict of interest. Dong Yang declares that he has no conflict of interest.

References

- Bellucci V., Flohr P., Paschereit C. O., and Magni F. (2004). On the use of helmholtz resonators for damping acoustic pulsations in industrial gas turbines. *Journal of Engineering for Gas Turbines and Power*. 126 (2): 271–275. <https://doi.org/10.1115/1.1473152>.
- Bourquard C. and Noiray N. (2019). Stabilization of acoustic modes using helmholtz and quarter-wave resonators tuned at exceptional points. *Journal of Sound and Vibration*. 445: 288–307. <https://doi.org/10.1016/j.jsv.2018.12.011>.
- Correa S. M. (1998). Power generation and aeropropulsion gas turbines: From combustion science to combustion technology. In Symposium (International) on Combustion, Vol. 27. Elsevier, pp. 1793–1807.
- Ćosić B., Wałmer D., Terhaar S., and Paschereit C. O. (2015). Acoustic response of helmholtz dampers in the presence of hot grazing flow. *Journal of Sound and Vibration*. 335: 1–18. <https://doi.org/10.1016/j.jsv.2014.08.025>.
- Dastourani H. and Bahman-Jahromi I. (2021). Evaluation of aeroacoustic performance of a helmholtz resonator system with different resonator cavity shapes in the presence of a grazing flow. *Journal of Aerospace Engineering*. 34 (5): 04021061. [https://doi.org/10.1061/\(ASCE\)AS.1943-5525.0001309](https://doi.org/10.1061/(ASCE)AS.1943-5525.0001309).
- Dupère I. D. J. and Dowling A. P. (2005). The use of helmholtz resonators in a practical combustor. *Journal of Engineering for Gas Turbines and Power*. 127 (2): 268–275. <https://doi.org/10.1115/1.1806838>.
- Eldredge J. D. and Dowling A. P. (2003). The absorption of axial acoustic waves by a perforated liner with bias flow. *Journal of Fluid Mechanics*. 485: 307–335. <https://doi.org/10.1017/S0022112003004518>.
- Gan Z., and Yang D. (2022). An acoustic analogy model for helmholtz resonators with cooling bias flow. *Chinese Journal of Theoretical and Applied Mechanics*. 54 (3): 1–11.
- Howe M. (1979). On the theory of unsteady high reynolds number flow through a circular aperture. *Proceedings of the Royal Society of London. A. Mathematical and Physical Sciences*. 366 (1725): 205–223. <https://doi.org/10.1098/rspa.1979.0048>.
- Lefebvre A. H., and Ballal D. R. (2010). Gas Turbine Combustion: Alternative Fuels and Emissions. Boca Raton, Florida: CRC Press.
- Lewis J. S., Niedzwiecki R. W., Bahr D., Bullock S., Cumpsty N., et al. (1999). Aircraft technology and its relation to emissions. In: *Aviation and the Global Atmosphere*. edited by: Jerry S. Lewis, Richard W. Niedzwiecki, DW Bahr, S Bullock, N Cumpsty, W Dodds, D DuBois, A Epstein, WW Freguson, A Fiorento and others. Cambridge: Cambridge University press, 291-70.
- Li J. and Morgans A. S. (2015). Time domain simulations of nonlinear thermoacoustic behaviour in a simple combustor using a wave-based approach. *Journal of Sound and Vibration*. 346: 345–360. <https://doi.org/10.1016/j.jsv.2015.01.032>.
- Lieuwen T. C. and Yang V. (2005). Combustion Instabilities in Gas Turbine Engines: Operational Experience, Fundamental Mechanisms, and Modeling: American Institute of Aeronautics and Astronautics. Reston, VA.
- Lu Z., Pan W., and Guan Y. (2019). Numerical studies of transmission loss performances of asymmetric helmholtz resonators in the presence of a grazing flow. *Journal of Low Frequency Noise, Vibration and Active Control*. 38 (2): 244–254. <https://doi.org/10.1177/1461348418817914>.
- Miniero L., Mensah G. A., Bourquard C., and Noiray N. (2023). Failure of thermoacoustic instability control due to periodic hot gas ingestion in helmholtz dampers. *Journal of Sound and Vibration*. 548: 117544. <https://doi.org/10.1016/j.jsv.2022.117544>.
- Palies P., Schuller T., Durox D., Gicquel L., and Candel S. (2011). Acoustically perturbed turbulent premixed swirling flames. *Physics of Fluids*. 23 (3): 037101. <https://doi.org/10.1063/1.3553276>.
- Poinsot T. (2017). Prediction and control of combustion instabilities in real engines. *Proceedings of the Combustion Institute*. 36 (1): 1–28. <https://doi.org/10.1016/j.proci.2016.05.007>.
- Royce R. (2015). *The jet engine*. John Wiley & Sons, London, England.
- Rupp J., Carrotte J., and Spencer A. (2010). Interaction between the acoustic pressure fluctuations and the unsteady flow field through circular holes. *Journal of Engineering for Gas Turbines and Power*. 132 (6), 205–216. <https://doi.org/10.1115/1.4000114>.
- Scarpato A., Tran N., Ducruix S., and Schuller T. (2012). Modeling the damping properties of perforated screens traversed by a bias flow and backed by a cavity at low strouhal number. *Journal of Sound and Vibration*. 331 (2): 276–290. <https://doi.org/10.1016/j.jsv.2011.09.005>.
- Selamet E., Selamet A., Iqbal A., and Kim H. (2011). Effect of flow on helmholtz resonator acoustics: A three-dimensional computational study vs. experiments, Technical report, SAE Technical Paper.
- Wu W. and Guan Y. (2021). Numerical investigation on low-frequency noise damping performances of helmholtz resonators with an extended neck in presence of a grazing flow. *Journal of Low Frequency Noise, Vibration and Active Control*. 40 (4): 2037–2053. <https://doi.org/10.1177/14613484211020584>.
- Yang D. and Morgans A. S. (2017). Acoustic models for cooled Helmholtz resonators. *AIAA Journal*. 55 (9): 3120–3127. <https://doi.org/10.2514/1.J055854>.
- Zheng M., Chen C., and Li X. (2023). The influence of the grazing flow and sound incidence direction on the acoustic characteristics of double helmholtz resonators. *Applied Acoustics*. 202: 109160. <https://doi.org/10.1016/j.apacoust.2022.109160>.